Check for updates

Hindawi
Journal of Mathematics
Volume 2023, Article ID 5527728, 14 pages
https://doi.org/10.1155/2023/5527728

Research Article

An Unconditionally Stable Difference Scheme for the Two-Dimensional Modified Fisher–Kolmogorov–Petrovsky–Piscounov Equation

Soobin Kwak, Seungyoon Kang, Seokjun Ham, Youngjin Hwang, Gyeonggyu Lee, and Junseok Kim

Department of Mathematics, Korea University, Seoul 02841, Republic of Korea

Correspondence should be addressed to Junseok Kim; cfdkim@korea.ac.kr

Received 18 January 2023; Revised 26 June 2023; Accepted 4 July 2023; Published 25 July 2023

Academic Editor: Sheng Du

Copyright © 2023 Soobin Kwak et al. This is an open access article distributed under the Creative Commons Attribution License, which permits unrestricted use, distribution, and reproduction in any medium, provided the original work is properly cited.

In this article, we develop an unconditionally stable numerical scheme for the modified Fisher–Kolmogorov–Petrovsky–Piscounov (Fisher–KPP) equation modeling population dynamics in two-dimensional space. The Fisher–KPP equation models the process of interaction between reaction and diffusion. The new solution algorithm is based on an alternating direction implicit (ADI) method and an interpolation method so that it is unconditionally stable. The proposed finite difference method is second-order accurate in time and space variables. Therefore, the main purpose of this study is to propose the novel Fisher–KPP equation with a nonlinear growth term and develop an unconditionally stable second-order numerical scheme. The novelty of our method is that it is a numerical method with second-order accuracy using interpolation and ADI methods in two dimensions. We demonstrate the performance of the proposed scheme through computational tests such as convergence and stability tests and the effects of model parameters and initial conditions.

1. Introduction

In this paper, we develop an unconditionally stable difference scheme for the modified Fisher–Kolmogorov–Petrovsky–Pisco unov (Fisher–KPP) equation in the two-dimensional (2D) space:

$$\frac{\partial u(x,y,t)}{\partial t} = D\Delta u(x,y,t) + K_{pq}u^p(x,y,t)[1-u(x,y,t)]^q, \quad (1)$$

where $u(x,y,t)$ is the population density at (x,y) in 2D domain Ω and at time t. Here D, K_{pq}, p, and q are all positive parameters. Figure 1 visualizes the reaction term, the second term $K_{pq}u^p(1-u)^q$ on the right side of equation (1), with various values of p and q.

To compare the difference depending on various values of p and q, we require its integral from 0 to 1 to be unit as shown in the following equation:

$$\int_0^1 K_{pq}u^p(1-u)^q du = 1, \quad (2)$$

where

$$K_{pq} = \frac{\Gamma(p+q+2)}{\Gamma(p+1)\Gamma(q+1)} \text{ and } \Gamma(z) = \int_0^\infty t^{z-1}e^{-t}\mathrm{d}t. \quad (3)$$

In this paper, unless otherwise stated, we use equation (3) for the value of K_{pq}.

The original equation, proposed by Fisher in a 1937 paper [1], is a one-dimensional model which has been studied in various forms. Salako and Shen studied the long time behaviour of random Fisher–KPP equation [2]. Tian et al. studied the Fisher–KPP with diffusion and nonlocal delay [3]. Leyva and Plaza focused on the spectral stability of the degenerate Fisher–KPP equation [4]. They investigated the long time behavior of solutions using numerical simulations. Hernández and Trofimchuk established the uniqueness of monotone wavefronts in the Fisher–KPP equation [5]. The Fisher–KPP equation has also been widely used in mathematical biology. Feng et al. proposed a single species movement model in a ranged boundary using the

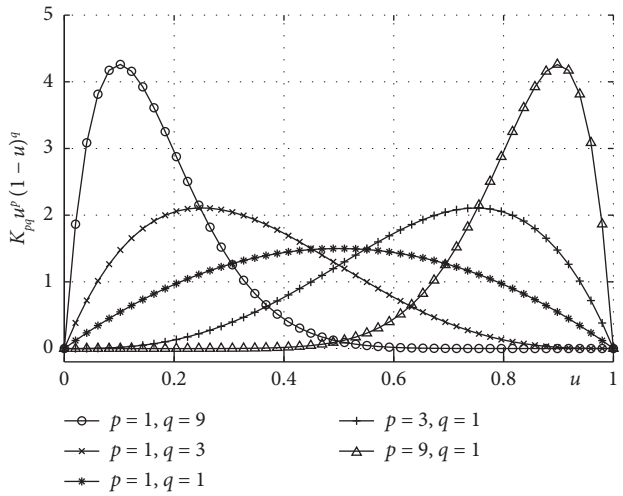

FIGURE 1: $K_{pq}u^p(1-u)^q$ with various p and q values.

Fisher–KPP equation [6]. Warne et al. presented a methodology that can be applied to various biological models, such as cell spreading [7]. In [8, 9], authors proposed entropy-based methods for the Fisher–KPP equation.

The Fisher–KPP equation has been expanded to include multidimensional equations. Roquejoffre and Roussier–Michon studied the asymptotic behaviour as time goes to infinity in two spatial dimensions [10]. Yahyaoui et al. used the 2D Fisher–KPP equation with time-dependent parameters to predict activated or inhibited cell-sheet wound closure [11]. In order to solve the 2D Fisher–KPP equation, Ozdemir et al. developed a three-step ultraspherical wavelet collocation method which is third-order accurate in time [12]. Their work is based on the Jacobi wavelet collocation method, which Secer and Cinar developed for the fractional Fisher's equation [13]. Rui and Zhang studied the Fisher–KPP type time-fractional reaction-diffusion models by combining the separation variable and integral bifurcation methods [14]. Time fractional Fisher–KPP is also studied by [15]. Furthermore, the finite difference method studied in [16] with the time fractional equation is applied in our proposed method. Minors and Dawes studied the dynamics of traveling wave solutions to the 2D Fisher–KPP equation [17]. Palencia analyzed a system including the Fisher–KPP reaction term, linear advection term, and high-order operator [18]. Attempts on three-and higher-order dimensions have also been made by Girardin [19]. Lou and Lu showed that the spreading phenomena in the high-dimensional Fisher–KPP equation converge to the unique positivity state [20]. They showed the uniqueness of the one-dimensional problem and used a different method for the N-dimensional problem. The gradient decay estimate for the solutions of the multidimensional Fisher–KPP equation was studied by Roquejoffre and Tarfulea [21]. They proved that the first and second derivatives of the solution decay exponentially over time. Flandoli et al. studied suitable conditions which can delay the blow-up by multiplicative noise in the three-dimensional Fisher–KPP equation [22]. Multidimensional Fisher–KPP equation was also used in describing a biological reaction-diffusion system. Khater and Alabdali used the nonlinear $(2+1)$-dimensional Fisher–KPP model in population genetics and nematic liquid crystals [23]. McCue et al. studied the porous-Fisher equation and its solutions' various properties [24]. Oruç solved the 2D Fisher–KPP equation using the Chebyshev wavelet method [25]. Faye and Holzer confirmed the nonlinear asymptotic stability of the critical front of the Fisher–KPP equation [26]. Xu et al. studied the nonlocal dispersal Fisher–KPP equation and considered three issues of spreading speed [27]. Furthermore, the various versions of the Fisher–KPP equation were studied [28–36]. In [28], the author considered the nonlocal diffusive Fisher model. They studied the problem of sudden jump points in a model. The authors in [29] considered a Fisher–KPP equation for the evolution of the spatial density of a single population. In [30], the authors considered the time fractional nonlinear KPP equation to investigate a mathematical biological model. They showed the condition of the existence and uniqueness of the governing equation. In addition, the numerical experiments showed practical solutions.

The main purpose of this study is to propose the novel Fisher–KPP equation with a nonlinear growth term and develop an unconditionally stable second-order numerical scheme. An important motivation for the proposed numerical scheme is to propose an operator splitting method (OSM) with second-order accuracy in both space and time using the interpolation method for the modified Fisher–KPP equation. The OSM has many advantages, such as reducing multidimensional problems to one-dimensional problems, simplifying problems, making unconditional schemes because they preserve order accuracy in time, and speeding up computations for some complex problems [37].

The paper is organized in the following way. In Section 2, we propose the numerical solution algorithm for the 2D Fisher–KPP equation. We present computational tests to confirm the effect of parameters, stability, and convergence of the proposed method in Section 3. In Section 4, the conclusion is given.

2. Numerical Solution Algorithm

We consider a 2D domain $\Omega = (L_x, R_x) \times (L_y, R_y)$ with an $N_x \times N_y$ grid to numerically solve equation (1). Let $h = (R_x - L_x)/N_x = (R_y - L_y)/N_y$ be the uniform spatial mesh size, Δt be time step, u_{ij}^n be an approximation of $u(x_i, y_j, t_n)$ at cell centers of the grid, where $x_i = L_x + (i - 0.5)h$ for $i = 1, 2, \ldots, N_x$, $y_j = L_y + (j - 0.5)h$ for $j = 1, 2, \ldots, N_y$, and $t_n = n\Delta t$. Let $\mathscr{L}(u(\mathbf{x}, t)) = D\Delta u(\mathbf{x}, t)$ be linear operator, $\mathscr{N}(u(\mathbf{x}, t)) = K_{pq}u^p(\mathbf{x}, t)[1 - u(\mathbf{x}, t)]^q$ be nonlinear operator, and $\mathbf{x} = (x, y)$ in 2D domain Ω. Thus, equation (1) can be written as follows:

$$\frac{\partial u(\mathbf{x}, t)}{\partial t} = \mathscr{L}(u(\mathbf{x}, t)) + \mathscr{N}(u(\mathbf{x}, t)). \tag{4}$$

To solve equation (4), we used the OSM [38]. The idea of OSM is to divide the operator of the system into simpler operators. Each operator can also be divided into fractional time steps. We divided the linear operator into two time

1469, 2023, 1, Downloaded from https://onlinelibrary.wiley.com/doi/10.1155/2023/5527728 by Junseok Kim - Korea University Medical , Wiley Online Library on [14/07/2025]. See the Terms and Conditions (https://onlinelibrary.wiley.com/terms-and-conditions) on Wiley Online Library for rules of use; OA articles are governed by the applicable Creative Commons License

steps, each progressing only a half time step $\Delta t/2$, whereas the nonlinear operator moves one full time step Δt. This makes our method be a second-order OSM. More specifically, we numerically solve equation (5) with $u_1(\mathbf{x},0) = u(\mathbf{x}, n\Delta t)$ to get $u_1(\mathbf{x}, \Delta t/2)$.

$$\frac{\partial u_1(\mathbf{x},t)}{\partial t} = \mathscr{L}\left(u_1(\mathbf{x},t)\right). \tag{5}$$

Using $u_1(\mathbf{x}, \Delta t/2)$, we numerically solve equation (6) with $u_2(\mathbf{x},0) = u_1(\mathbf{x}, \Delta t/2)$ to get $u_2(\mathbf{x}, \Delta t)$.

$$\frac{\partial u_2(\mathbf{x},t)}{\partial t} = \mathscr{N}\left(u_2(\mathbf{x},t)\right). \tag{6}$$

Using $u_2(\mathbf{x}, \Delta t)$, we numerically solve equation (7) with $u_3(\mathbf{x},0) = u_2(\mathbf{x}, \Delta t)$ to get $u_3(\mathbf{x}, \Delta t/2)$.

$$\frac{\partial u_3(\mathbf{x},t)}{\partial t} = \mathscr{L}\left(u_3(\mathbf{x},t)\right). \tag{7}$$

Finally, we set $u(\mathbf{x}, (n+1)\Delta t) = u_3(\mathbf{x}, \Delta t/2)$. The full scheme is as follows:

$$u(\mathbf{x}, (n+1)\Delta t) = \left(\mathscr{L}^{\Delta t/2} \circ \mathscr{N}^{\Delta t} \circ \mathscr{L}^{\Delta t/2}\right) u(\mathbf{x}, n\Delta t). \tag{8}$$

Equations (5) and (7) can be solved using the alternating directions implicit (ADI) finite difference method [39]. Now, we introduce the ADI method. The ADI method solves an equation by dividing a time step into two stages. Here, each stage treats only one operator implicitly and uses a half time step. We solve the equation with each standard space direction. The equation is first implicitly solved with respect to x and then implicitly solved with respect to y in 2D. For simplicity, we denote u_1 and u_3 by u.

$$\frac{u_{ij}^* - u_{ij}^n}{\Delta t/2} = \mathscr{L}_{\mathrm{ADI}}^x u_{ij}^*, \tag{9}$$

$$\frac{u_{ij}^{**} - u_{ij}^*}{\Delta t/2} = \mathscr{L}_{\mathrm{ADI}}^y u_{ij}^{**}, \tag{10}$$

with discrete difference operators $\mathscr{L}_{\mathrm{ADI}}^x$ and $\mathscr{L}_{\mathrm{ADI}}^y$ defined by

$$\begin{aligned}
\mathscr{L}_{\mathrm{ADI}}^x u_{ij}^* &= \frac{D}{2}\frac{u_{i+1,j}^* - 2u_{ij}^* + u_{i-1,j}^*}{h^2} + \frac{D}{2}\frac{u_{i,j+1}^n - 2u_{ij}^n + u_{i,j-1}^n}{h^2}, \\
\mathscr{L}_{\mathrm{ADI}}^y u_{ij}^{**} &= \frac{D}{2}\frac{u_{i+1,j}^* - 2u_{ij}^* + u_{i-1,j}^*}{h^2} + \frac{D}{2}\frac{u_{i,j+1}^{**} - 2u_{ij}^{**} + u_{i,j-1}^{**}}{h^2}.
\end{aligned} \tag{11}$$

Adding equations (9) and (10), we get the following equation:

$$\frac{u_{ij}^{**} - u_{ij}^n}{\Delta t/2} = \mathscr{L}_{\mathrm{ADI}}^x u_{ij}^* + \mathscr{L}_{\mathrm{ADI}}^y u_{ij}^{**}. \tag{12}$$

After finding $u_1(\mathbf{x}, \Delta t/2)$ by solving the diffusion equation with ADI method, we use a recently developed interpolation method [41, 42] to solve the nonlinear equation (6). Assume that M is a fixed positive integer. Let $I = \{I_s \mid I_s = (s-1)/(M-1), \text{for } s = 1, \ldots, M\}$ be a partition of the unit interval. We numerically solve equation (6) on the grid I with a smaller time step $\Delta\tau = \Delta t/N_\tau$ where N_τ will be later defined. Because equation (6) is an ordinary differential equation with respect to time variable t with fixed values of spatial variable (x, y), we can rewrite it with a new variable $\Phi(t)$:

$$\frac{d\Phi(t)}{dt} = K_{pq}\Phi^p(t)[1 - \Phi(t)]^q. \tag{13}$$

Let $\Phi_s(t)$ be the function satisfying equation (13) for $s = 1, \ldots, M$ with the initial condition $\Phi_s(0) = I_s$. To simplify, we use an explicit Euler's method, which is for each $m = 0, \ldots, N_\tau - 1$,

$$\Phi_s((m+1)\Delta\tau) = \Phi_s(m\Delta\tau) + \Delta\tau K_{pq}\Phi_s^p(m\Delta\tau)\left(1 - \Phi_s(m\Delta\tau)\right)^q. \tag{14}$$

Therefore, we obtain the numerical solution $\Phi_s(\Delta t)$ of equation (14) at the point I_s, as shown in Figure 2.

Next, we compute an N_τ which can stably integrate equation (14). If $I_s = 0$ or 1, then for any $\Delta\tau$,

$$\Phi_s((m+1)\Delta\tau) = I_s, \quad \text{for } m = 0, \ldots, N_\tau - 1, \tag{15}$$

from equation (14). We want to say that $\Phi_s((m+1)\Delta\tau)$ is bounded by zero and one for $m = 0, \ldots, N_\tau - 1$ when $0 < I_s < 1$. We can show $0 \le \Phi_s((m+1)\Delta\tau) \le 1$ from the former step $0 \le \Phi_s(\Delta\tau) \le 1$ using the mathematical induction. Assume that $0 < I_s < 1$, $\Phi_s(0) = I_s$, and $m = 0$. Then by equation (14) we get

$$\Phi_s(\Delta\tau) = I_s + \Delta\tau K_{pq} I_s^p (1 - I_s)^q. \tag{16}$$

We have $\Phi_s(\Delta\tau) > 0$ for any $\Delta\tau$ from equation (16) because $K_{pq} I_s^p (1 - I_s)^q > 0$ for $0 < I_s < 1$. Therefore, we only need to find $\Delta\tau$ satisfying $\Phi_s(\Delta\tau) \le 1$, i.e., $I_s + \Delta\tau K_{pq} I_s^p (1 - I_s)^q \le 1$, which results in the inequality

$$\Delta\tau \le I_s^{-p}\left(1 - I_s\right)^{1-q}/K_{pq}. \tag{17}$$

Let $G(I_s) = I_s^{-p}(1 - I_s)^{1-q}/K_{pq}$ be the right hand side of equation (17). The critical value of $G(I_s)$ on $0 < I_s < 1$ is $I_s = p/(p+q-1)$ because $G'(I_s) = I_s^{-p-1}(1 - I_s)^{-q}[(p+q-1)I_s - p]/K_{pq}$. If we assume $p, q \ge 1$, then we have two cases: $0 < p/(p+q-1) < 1$ and $p/(p+q-1) \ge 1$, as shown in Figures 3(a) and 3(b), respectively.

In the case of $0 < p/(p+q-1) < 1$, $\Delta\tau = I_*^{-p}(1 - I_*)^{1-q}/K_{pq}$ satisfies equation (17), where $I_* = p/(p+q-1)$. Therefore, we set $N_\tau = [\Delta t I_*^p (1 - I_*)^{q-1} K_{pq}] + 1$, where $[x]$ is the floor function. In the case of $q \le 1$, which implies $q = 1$ because we assumed $q \ge 1$. Then, $G(I_s) = I_s^{-p}/K_{pq}$ becomes a decreasing function and $\Delta\tau = 1/K_{pq}$ satisfies equation (17) for any I_s. Therefore, we set $N_\tau = [\Delta t K_{pq}] + 1$. In summary, we have the following formula:

$$N_\tau = \begin{cases} \left[\Delta t K_{pq}\right] + 1, & \text{if } q = 1, \\ \left[\Delta t I_*^p (1 - I_*)^{q-1} K_{pq}\right] + 1, & \text{if } q > 1, \end{cases} \tag{18}$$

where $I_* = p/(p+q-1)$. Now, with precomputed numerical solutions $\Phi_s(\Delta t)$ for $s = 1, \ldots, M$ and u_{ij}^{**}, we

1469, 2023, 1, Downloaded from https://onlinelibrary.wiley.com/doi/10.1155/2023/5527728 by Junseok Kim - Korea University Medical , Wiley Online Library on [14/07/2025]. See the Terms and Conditions (https://onlinelibrary.wiley.com/terms-and-conditions) on Wiley Online Library for rules of use; OA articles are governed by the applicable Creative Commons License

(i) Step 1: equation (9) is rewritten as

$$\alpha_i u^*_{i-1,j} + \beta_i u^*_{ij} + \gamma_i u^*_{i+1,j} = f^n_{ij},$$

where

$$\alpha_i = -D/(2h^2), \beta_i = 2/\Delta t + D/h^2, \gamma_i = -D/(2h^2),$$
$$f^n_{ij} = 2u^n_{ij}/\Delta t + D(u^n_{i,j+1} - 2u^n_{ij} + u^n_{i,j-1})/(2h^2).$$

For a fixed index j, the solution vector $u^*_{1:N_x,j}$ is found by solving the tridiagonal system [40]

$$A_x u^*_{1:N_x,j} = f^n_{1:N_x,j},$$

where

$$A_x = \begin{pmatrix} \beta_1 + \alpha_1 & \gamma_1 & 0 & \dots & 0 & 0 \\ \alpha_2 & \beta_2 & \gamma_2 & \dots & 0 & 0 \\ 0 & \alpha_3 & \beta_3 & \dots & 0 & 0 \\ \vdots & \vdots & \ddots & \ddots & \ddots & \vdots \\ 0 & 0 & 0 & \dots & \beta_{N_x-1} & \gamma_{N_x-1} \\ 0 & 0 & 0 & \dots & \alpha_{N_x} & \beta_{N_x} + \gamma_{N_x} \end{pmatrix}.$$

Then, we perform a loop over the y-direction:

```
for j = 1: N_y
    for i = 1: N_x
        set α_i, β_i, γ_i, and f^n_ij by equations (Algorithm 1)
    end
    Solve A_x u*_{1:N_x,j} = f^n_{1:N_x,j} by using the Thomas algorithm
end
```

(ii) Step 2: equation (10) is rewritten as

$$\alpha_j u^{**}_{i,j-1} + \beta_j u^{**}_{ij} + \gamma_j u^{**}_{i,j+1} = g^*_{ij},$$

where

$$\alpha_j = -D/(2h^2), \beta_j = 2/\Delta t + D/h^2, \gamma_j = -D/(2h^2),$$
$$g^*_{ij} = 2u^*_{ij}/\Delta t + D(u^*_{i+1,j} - 2u^*_{ij} + u^*_{i-1,j})/(2h^2).$$

For a fixed index i, the solution vector $u^{**}_{i,1:N_y}$ is found by solving the tridiagonal system

$$A_y u^{**}_{i,1:N_y} = g^*_{i,1:N_y},$$

where

$$A_y = \begin{pmatrix} \beta_1 + \alpha_1 & \gamma_1 & 0 & \dots & 0 & 0 \\ \alpha_2 & \beta_2 & \gamma_2 & \dots & 0 & 0 \\ 0 & \alpha_3 & \beta_3 & \dots & 0 & 0 \\ \vdots & \vdots & \ddots & \ddots & \ddots & \vdots \\ 0 & 0 & 0 & \dots & \beta_{N_y-1} & \gamma_{N_y-1} \\ 0 & 0 & 0 & \dots & \alpha_{N_y} & \beta_{N_y} + \gamma_{N_y} \end{pmatrix}.$$

Then, we perform a loop over the x-direction:

```
for i = 1: N_x
    for j = 1: N_y
        set α_j, β_j, γ_j, and g*_ij by equations (Algorithm 1)
    end
    solve A_y u**_{i,1:N_y} = g*_{i,1:N_y} by using the Thomas algorithm
end
```

Algorithm 1: ADI.

calculate u^{***}_{ij} using the piecewise linear interpolation as follows:

$$u^{***}_{ij} = \frac{I_{s+1} - u^{**}_{ij}}{I_{s+1} - I_s}\Phi_s(\Delta t) + \frac{u^{**}_{ij} - I_s}{I_{s+1} - I_s}\Phi_{s+1}(\Delta t), \tag{19}$$

where $I_s \le u^{**}_i \le I_{s+1}$ for some s. As abovementioned, u^{**}_{ij} is $u_1(x_i, y_j, n\Delta t)$ and u^{***}_{ij} is $u_2(x_i, y_j, \Delta t)$. Finally, we can get $u_3(x_i, y_j, \Delta t/2)$ using the ADI method and $u_2(x_i, y_j, \Delta t)$. We illustrated u^{n+1}_{ij} schematically in Figure 4.

The stability and convergence of the proposed method are as follows. The proposed algorithm consists of the three steps, i.e., equations (5)–(7). In the first step, equation (5) is the two-dimensional partial differential equation.

$$\frac{\partial u(x,y,t)}{\partial t} = \frac{\partial^2 u(x,y,t)}{\partial x^2} + \frac{\partial^2 u(x,y,t)}{\partial y^2}, \tag{20}$$

which is numerically solved in equations (9) and (10) by using the Peaceman–Rachford (PR) ADI method [39]. This ADI scheme was proved unconditionally stable in [39]. In the second step, equation (6) is the nonlinear equation as follows:

$$\frac{\partial u(x,y,t)}{\partial t} = K_{pq} u^p(x,y,t)[1 - u(x,y,t)]^q, \tag{21}$$

which is solved using the interpolation. Its numerical solution, given by equation (19), is unconditionally stable from the construction of the scheme. In the third step, equation (7) is the same to equation (5). The numerical solution for

1469, 2023, 1, Downloaded from https://onlinelibrary.wiley.com/doi/10.1155/2023/5527728 by Junseok Kim - Korea University Medical , Wiley Online Library on [14/07/2025]. See the Terms and Conditions (https://onlinelibrary.wiley.com/terms-and-conditions) on Wiley Online Library for rules of use; OA articles are governed by the applicable Creative Commons License

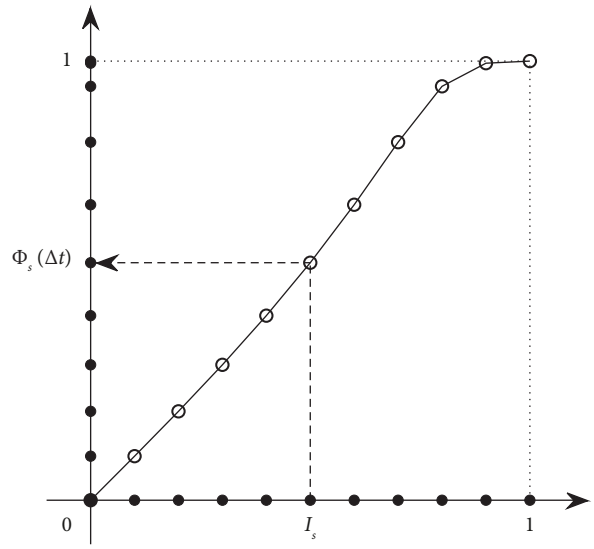

FIGURE 2: Numerical solution $\Phi_s(\Delta t)$ of equation (16) at the point I_s.

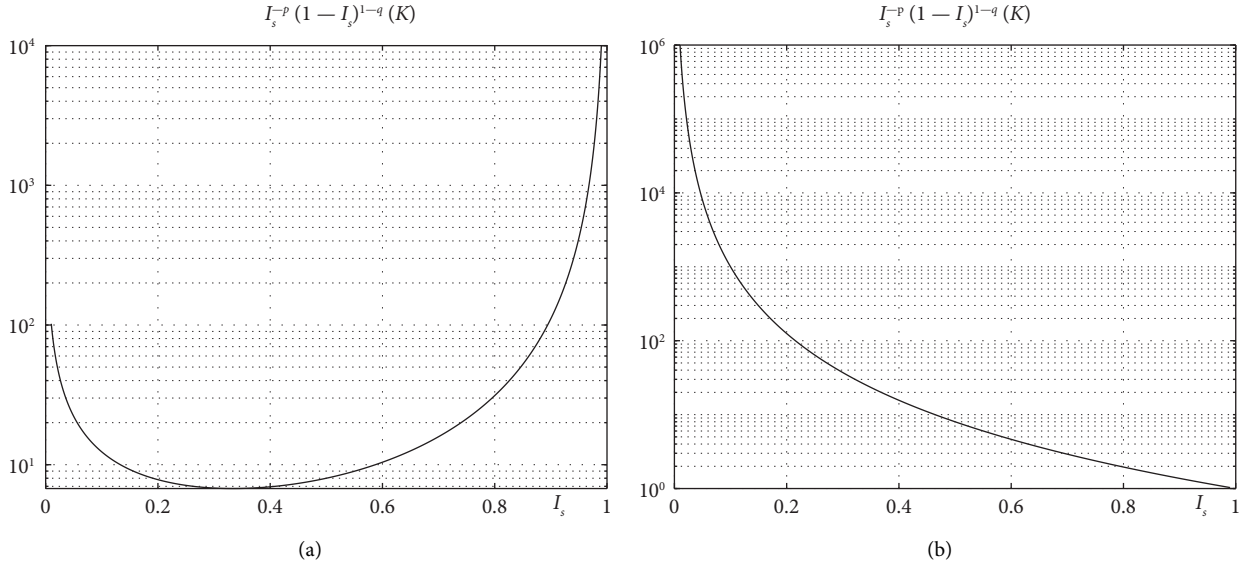

FIGURE 3: Semilogy plot of $G(I_s) = I_s^{-p}(1-I_s)^{1-q}/K_{pq}$ with respect to I_s: (a) $p = 1, q = 3$ and (b) $p = 3, q = 1$.

the third step is also unconditionally stable. Therefore, the proposed numerical scheme is unconditionally stable because all substeps are unconditionally stable.

Next, we consider the convergence of the proposed method. In the first and third steps, the ADI scheme is temporally and spatially second-order accurate, as proved in [39]. Due to the property of time subcycling in the second step, we can make the scheme second-order accurate. As described in [43], the full scheme (8) is temporally and spatially second-order accurate.

In this study, for the sake of presentation, we presented the proposed method in rectangular space domains discretized with Cartesian meshes and uniform discretization of the time interval. If complex space domains are used, then it is better to use other methods such as the multigrid method [44] for the heat equation part. For a more efficient method, we may use the adaptive time step method.

3. Computational Tests

3.1. Convergence Tests. We use the initial condition of equation (1) in $\Omega = (-20, 20) \times (-20, 20)$ with $D = K_{pq} = p = q = 1$ as follows:

$$u(x, y, 0) = \left[\frac{1}{2} - \frac{1}{2}\tanh\left(\frac{x}{2\sqrt{6}}\right)\right]^2. \tag{22}$$

The exact solution is given in [41]:

$$u(x, y, t) = \left[\frac{1}{2} - \frac{1}{2}\tanh\left(\frac{x}{2\sqrt{6}} - \frac{5t}{12}\right)\right]^2. \tag{23}$$

Figure 5 shows $u(x, y, 0)$ (gray color) and $u(x, y, 4)$ (transparent color).

1469, 2023, 1, Downloaded from https://onlinelibrary.wiley.com/doi/10.1155/2023/5527728 by Junseok Kim - Korea University Medical , Wiley Online Library on [14/07/2025]. See the Terms and Conditions (https://onlinelibrary.wiley.com/terms-and-conditions) on Wiley Online Library for rules of use; OA articles are governed by the applicable Creative Commons License

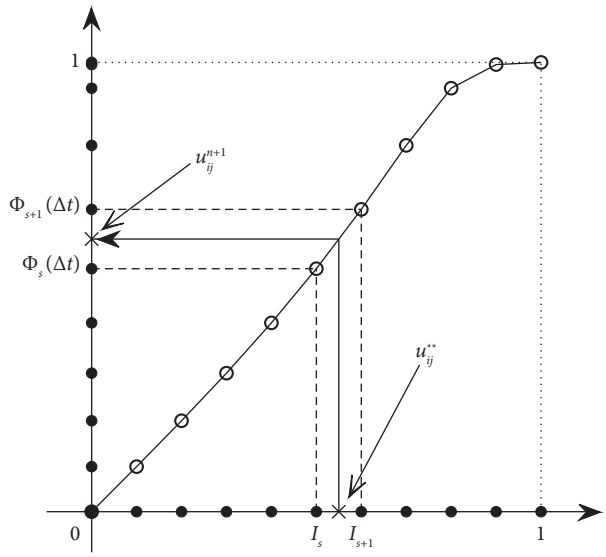

Figure 4: Schematic diagram of u_{ij}^{n+1} using the interpolation.

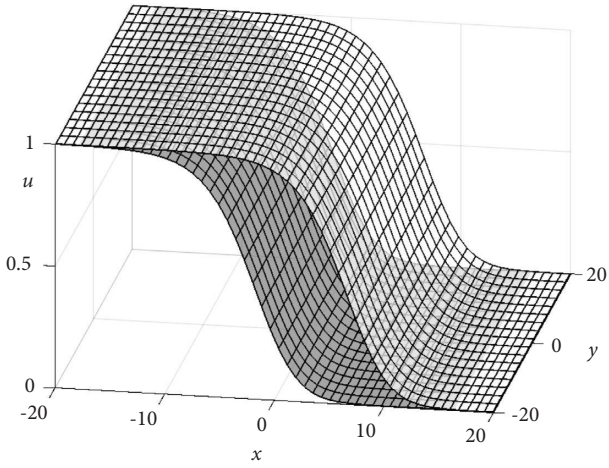

Figure 5: $u(x, y, 0)$ (gray color) and $u(x, y, 4)$ (transparent color).

Table 1: l_2-norm error and temporal convergence rate.

N_t	64	128	256	512
Error (N_t)	2.6764e − 03	6.7565e − 04	1.6887e − 04	4.2921e − 05
Rate $(N_t, 2N_t)$	1.9859	2.0004	1.9762	
CPU time (s)	0.3011	0.5894	1.1635	2.3023

Table 2: l_2-norm error and spatial convergence rate.

$N_x \times N_y$	16×16	32×32	64×64	128×128
Error $(N_x \times N_y)$	2.9605e − 03	7.6411e − 04	1.8824e − 04	4.3929e − 05
Rate $(N_x \times N_y, 2N_x \times 2N_y)$	1.9540	2.0212	2.0994	
CPU time (s)	2.2735	5.1009	14.5456	43.7526

We list the l_2-norm error between the proposed numerical and exact solutions, and the convergence rate of the numerical results of increasing N_t values with fixed final time $T = 4$ and $N_x = N_y = 2^8$ in Table 1. (i.e., Rate $(N_t, 2N_t) = \log(\text{Error}(N_t)/\text{Error}(2N_t))/\log(2))$. Here, l_2-norm error is defined as follows:

1469, 2023, 1, Downloaded from https://onlinelibrary.wiley.com/doi/10.1155/2023/5527728 by Junseok Kim - Korea University Medical , Wiley Online Library on [14/07/2025]. See the Terms and Conditions (https://onlinelibrary.wiley.com/terms-and-conditions) on Wiley Online Library for rules of use; OA articles are governed by the applicable Creative Commons License

$$(l_2\text{-norm error}) = \sqrt{\frac{1}{N_x N_y}\sum_{i=1}^{N_x}\sum_{j=1}^{N_y}\left(u_{ij}^{\text{exact}} - u_{ij}\right)^2}, \quad (24)$$

where u^{exact} is the exact solution of u. Therefore, we can confirm that the computational method is second-order accurate in time.

We list the l_2-norm error between the proposed numerical and exact solutions, and the convergence rate of the numerical results of increasing $N_x \times N_y$ values with fixed final time $T = 4$ and $N_t = 2^{15}$ in Table 2. (i.e., Rate $(N_x \times N_y, 2N_x \times 2N_y) = \log(\text{Error } (N_x \times N_y)/\text{Error}\,(2N_x \times 2N_y))/\log(2))$. Therefore, we can confirm that the computational method is second-order accurate in space.

Tables 1 and 2 provide CPU times calculated using an Intel(R) Core(TM) i9-13900K 3.00 GHz processor for each experiment.

3.2. Stability Test. We perform that the proposed method is unconditionally stable. We use the initial condition (22) to check whether the proposed scheme is stable on $\Omega = (-20, 80) \times (-0.5, 0.5)$. The parameters are $N_x = 1000$, $N_y = 10$, and $T = 30$. We examine three different time steps $\Delta t = 0.01$, 0.1, and 1. In Figure 6, for $\Delta t = 0.01$, it is confirmed that the result overlaps with the exact solution equation (23). The solution does not blow up for $\Delta t = 1$.

3.3. D Effects. We simulate the computational test to observe the effect of the diffusion coefficient D. The initial conditions are as follows:

$$u(x, y, 0) = 0.2\cos(2\pi x)\cos(2\pi y) + C, \quad (25)$$

where C is constant, $N_x = N_y = 100$, $T = 0.4$, $\Delta t = 0.01$, and $p = q = 1$ on $\Omega = (0, 1) \times (0, 1)$. Figure 7 shows the effect of diffusion coefficient D with (a) $C = 0.25$, (b) $C = 0.5$, and (c) $C = 0.75$. From the top to bottom rows, initial condition (24), result with $D = 0.001$, result with $D = 0.1$, and temporal evolution of total mass M are shown. We can observe that the case of $D = 0.1$ flattened faster than the case of $D = 0.001$. With $C = 0.25$, as shown in Figure 7(a), the temporal evolution of the total mass is greater with $D = 0.1$ than $D = 0.001$.

3.4. p and q Effects. We investigate the effect of p and q values with the following initial condition on $\Omega = (0, 1) \times (0, 1)$:

$$u(x, y, 0) = 0.45\cos(2\pi x)\cos(2\pi y) + 0.5. \quad (26)$$

We also calculate and observe M, defined as the total mass. The parameters are $N_x = N_y = 100$, $\Delta t = 0.01$, and $D = 0.001$. Here, a small diffusion coefficient D is used to minimize the diffusion term effect and make the nonlinear term dominant in equation (1). This section is divided into two parts: $p = q$ and $p \neq q$.

3.4.1. $p = q$. For $p = q$, Figure 8 shows the profiles of $K_{pq}u^p(1-u)^q$ with $p = q =$ 1,2,5, and 10. As the values of p and q increase, the curve of $K_{pq}u^p(1-u)^q$ becomes narrower around $u = 0.5$.

In Figure 9, (a) is the initial condition (25), and (b) is the temporal evolution of each total mass M with $p = q = 1$ (solid line) and $p = q = 10$ (dashed line). We can observe the reversion of the total mass as time evolves. In early times, the total mass with $p = q = 10$ is larger, however, later the total mass with $p = q = 1$ is larger. (c) and (d) are profiles of $u(x, y, t)$ with $p = q = 1$ and $p = q = 10$, respectively. (e) is the subtraction (d) from (c). Here, the gray plane is the plane where $z = 0$. From the left to right column, $t = 0.05$, 0.1, and 1.5, respectively. As shown in Figure 9(e), we can observe that in the case of $p = q = 1$, the small concentration of mass grows faster than the other case.

3.4.2. $p \neq q$. In Figure 10, (a) is the initial condition (25), (b) is the temporal evolution of each total mass M with $p = 1$, $q = 9$ (dashed line); $p = q = 5$ (solid line); and $p = 9$, $q = 1$ (dotted line). We can observe different increases of the total mass as time evolves. (c), (d), and (e) are profiles of $u(x, y, t)$ with $p = 1$, $q = 9$; $p = q = 5$; and $p = 9$, $q = 1$, respectively. From left to right column, $t = 0.2$, 0.4, and 0.6, respectively.

3.5. Evolution of Numerical Solution. Next, we consider the effect of initial configuration on the evolution. We use three different initial conditions on $\Omega = (-1.2, 1.2) \times (-1.2, 1.2)$:

$$u(x, y, 0) = \begin{cases} 0.2, & \text{if } -0.57 \le x \le 0.61, \\ 0, & \text{otherwise,} \end{cases} \quad (27)$$

$$u(x, y, 0) = \begin{cases} 0.2, & \text{if } -0.97 + 0.8k \le x \le -0.59 + 0.8k \text{ for } k = 0,\ 1,\ 2, \\ 0, & \text{otherwise,} \end{cases} \quad (28)$$

$$u(x, y, 0) = \begin{cases} 0.2, & \text{if } -1.07 + 0.4k \le x \le -0.89 + 0.4k \text{ for } k = 0, \ldots, 5, \\ 0, & \text{otherwise.} \end{cases} \quad (29)$$

1469, 2023, 1, Downloaded from https://onlinelibrary.wiley.com/doi/10.1155/2023/5527728 by Junseok Kim - Korea University Medical , Wiley Online Library on [14/07/2025]. See the Terms and Conditions (https://onlinelibrary.wiley.com/terms-and-conditions) on Wiley Online Library for rules of use; OA articles are governed by the applicable Creative Commons License

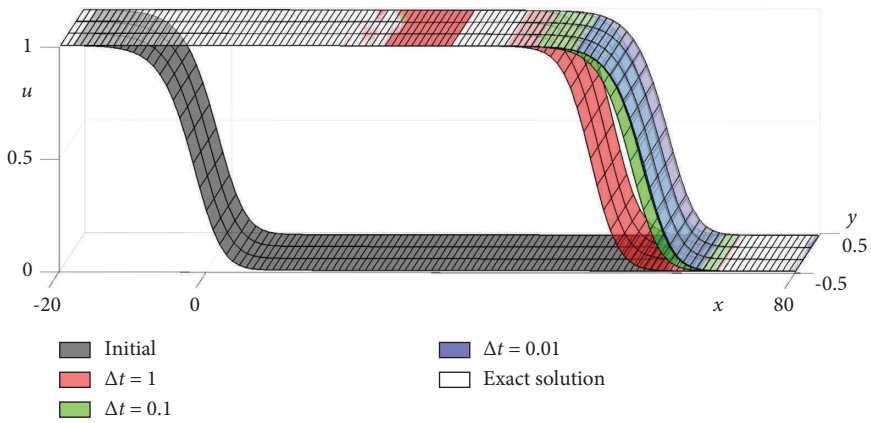

Figure 6: Numerical solutions using $\Delta t = 0.01$, 0.1, 1, and exact solution.

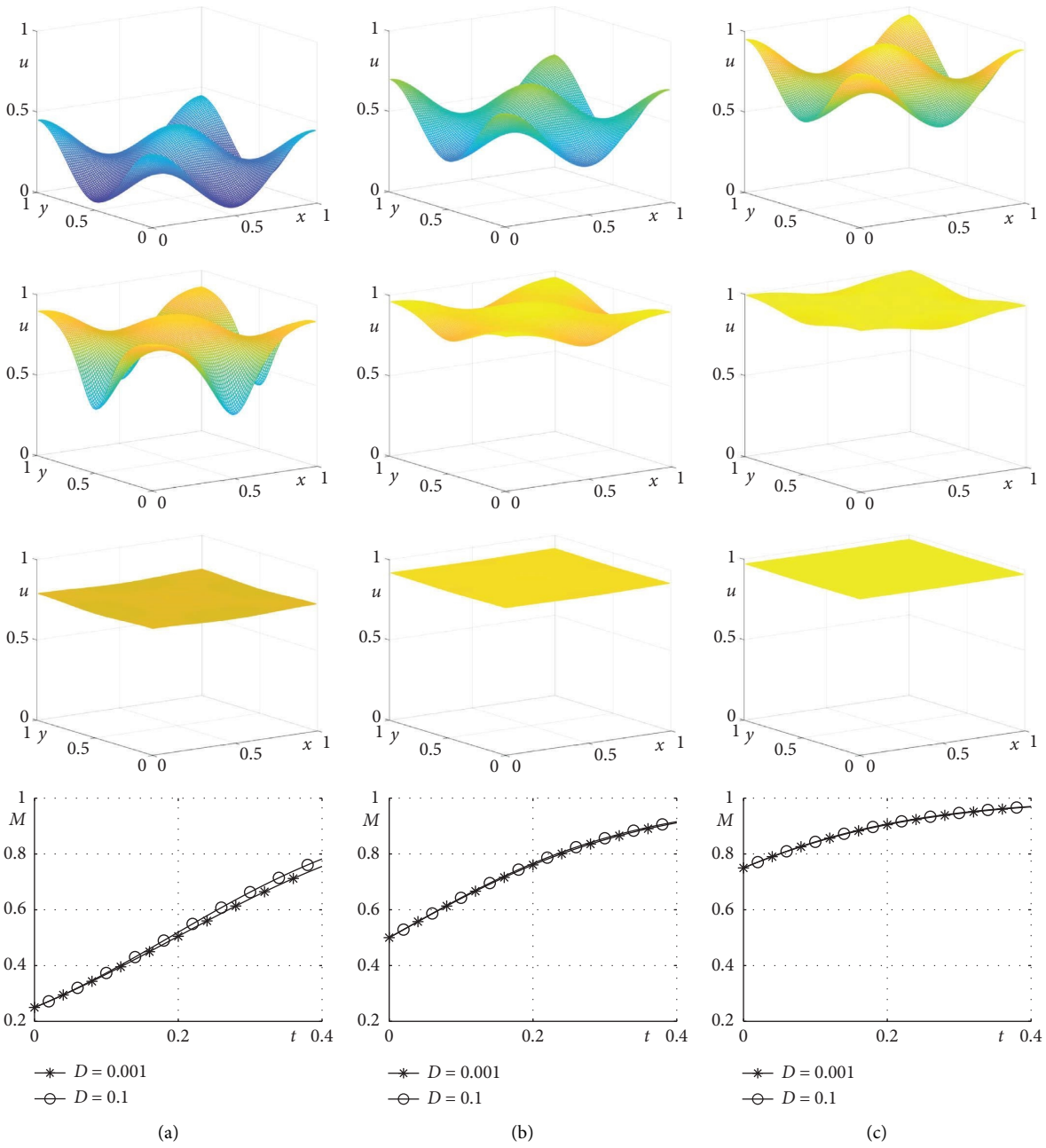

Figure 7: Effect of diffusion coefficient D: (a) $C = 0.25$, (b) $C = 0.5$, and (c) $C = 0.75$. From to bottom rows, initial condition (24), result with $D = 0.001$, result with $D = 0.1$, and temporal evolution of total mass.

1469, 2023, 1, Downloaded from https://onlinelibrary.wiley.com/doi/10.1155/2023/5527728 by Junseok Kim - Korea University Medical , Wiley Online Library on [14/07/2025]. See the Terms and Conditions (https://onlinelibrary.wiley.com/terms-and-conditions) on Wiley Online Library for rules of use; OA articles are governed by the applicable Creative Commons License

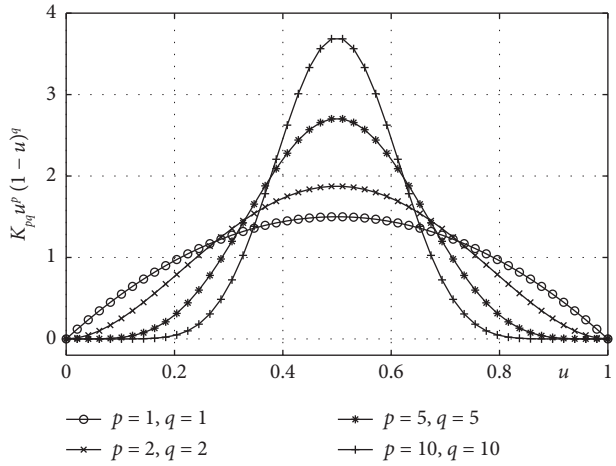

Figure 8: Profiles of $K_{pq}u^p(1-u)^q$ with $p = q = 1, 2, 5$, and 10.

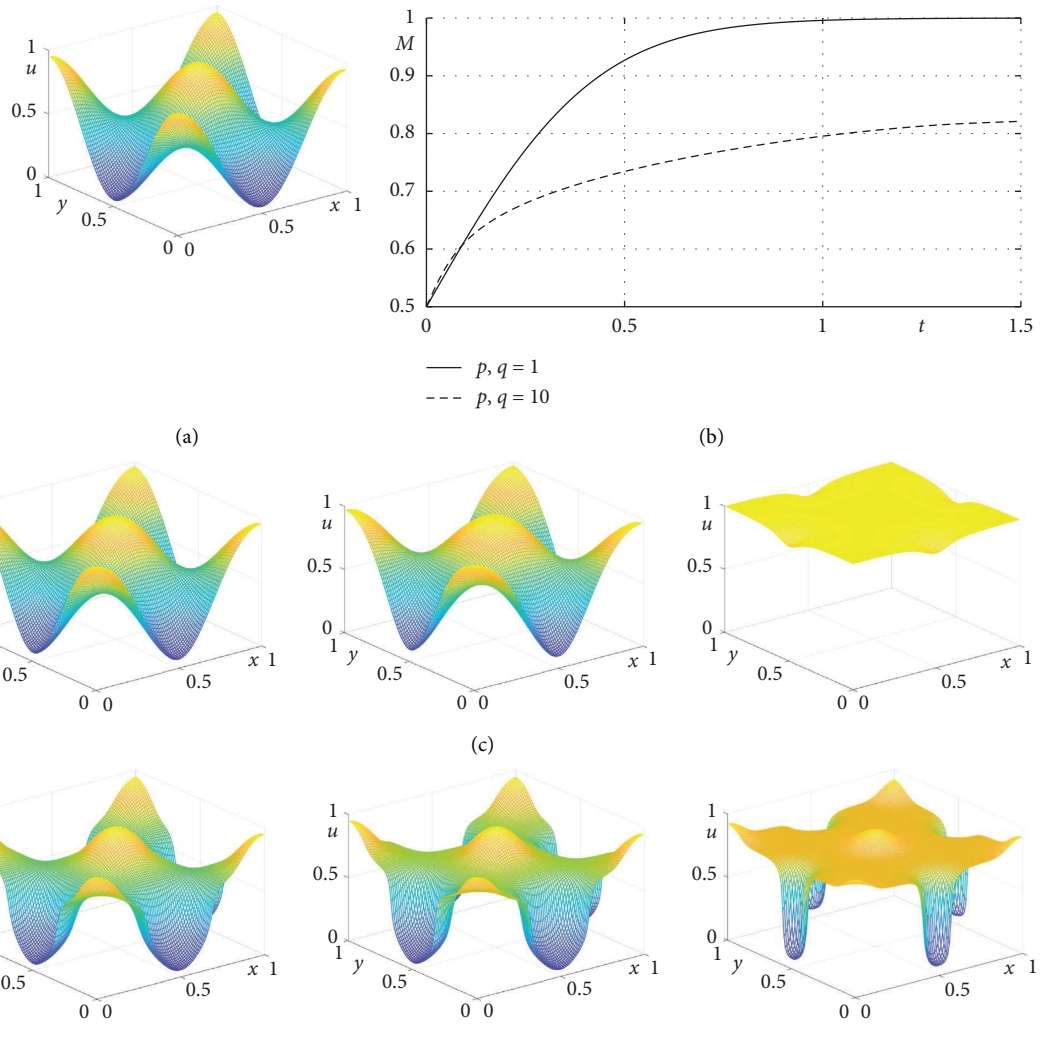

Figure 9: Continued.

1469, 2023, 1, Downloaded from https://onlinelibrary.wiley.com/doi/10.1155/2023/5527728 by Junseok Kim - Korea University Medical , Wiley Online Library on [14/07/2025]. See the Terms and Conditions (https://onlinelibrary.wiley.com/terms-and-conditions) on Wiley Online Library for rules of use; OA articles are governed by the applicable Creative Commons License

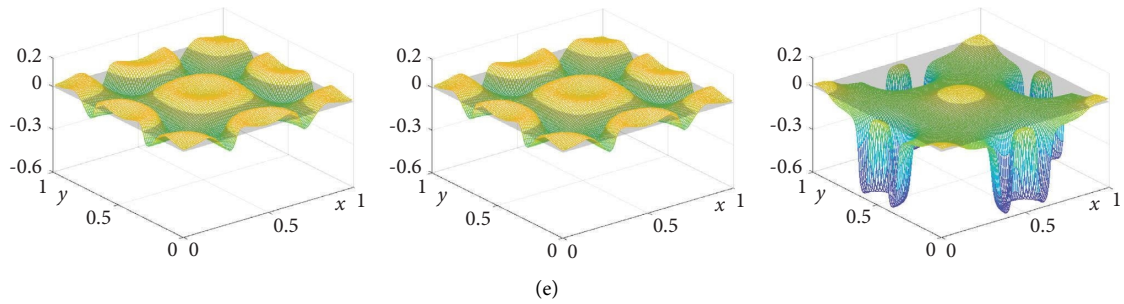

Figure 9: (a) Initial condition $(t = 0)$. (b) Temporal evolution of each total mass with $p = q = 1$ (solid line) and $p = q = 10$ (dashed line). Configurations of $u(x, y, t)$ with (c) $p = q = 1$ and (d) $p = q = 10$. (e) Subtraction (d) from (c). From left to right column, $t = 0.05$, 0.1, and 1.5, respectively.

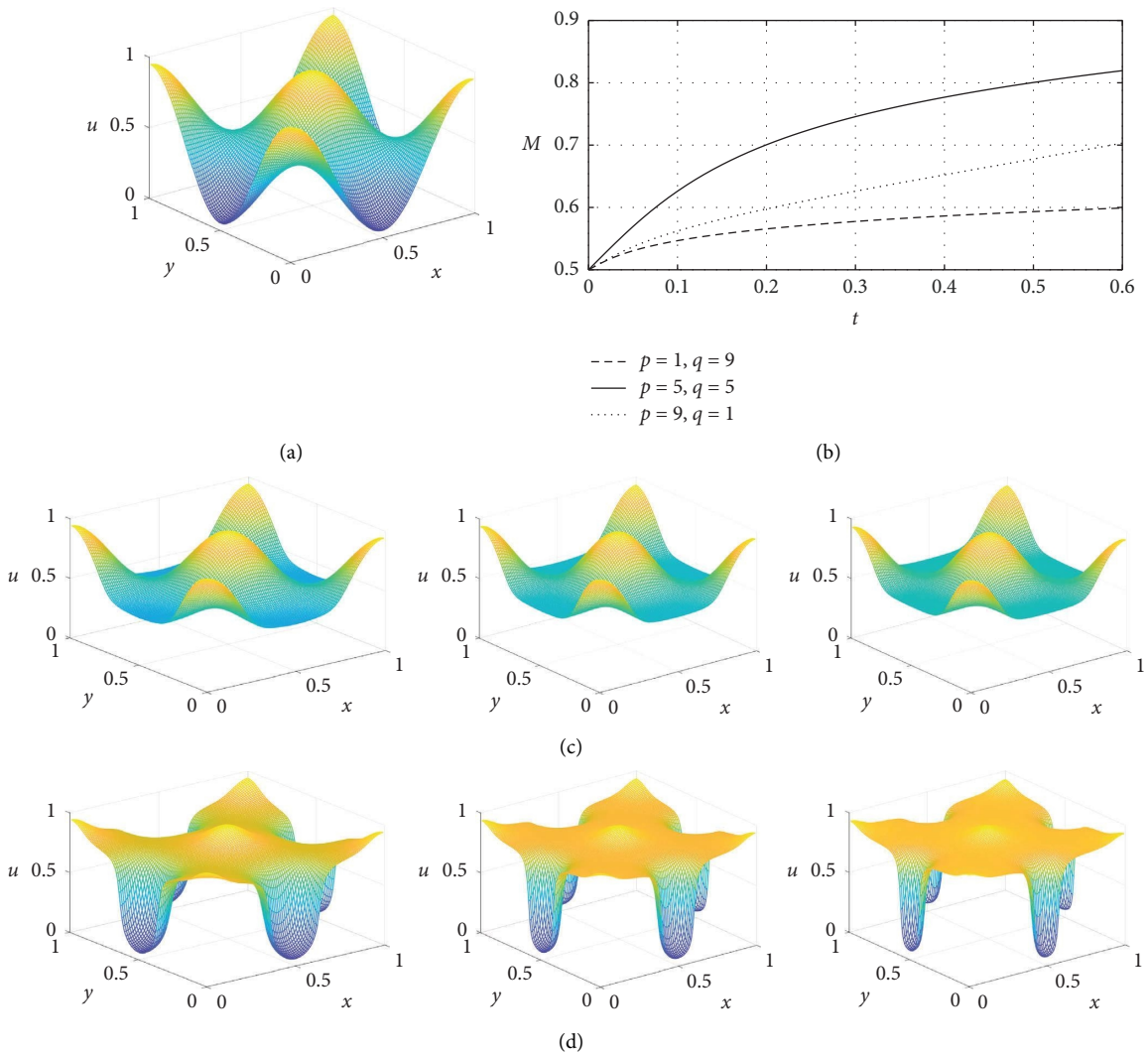

Figure 10: Continued.

1469, 2023, 1, Downloaded from https://onlinelibrary.wiley.com/doi/10.1155/2023/5527728 by Junseok Kim - Korea University Medical , Wiley Online Library on [14/07/2025]. See the Terms and Conditions (https://onlinelibrary.wiley.com/terms-and-conditions) on Wiley Online Library for rules of use; OA articles are governed by the applicable Creative Commons License

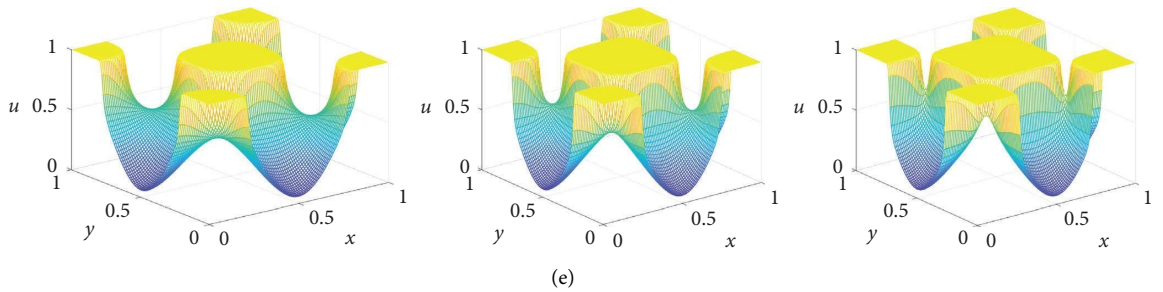

(e)

Figure 10: (a) Initial condition $(t = 0)$. (b) Temporal evolution of each total mass with $p = 1, q = 9$ (dashed line); $p = q = 5$ (solid line); and $p = 9, q = 1$ (dotted line). Configurations of $u(x, y, t)$ with (c) $p = 1, q = 9$; (d) $p = q = 5$; and (e) $p = 9, q = 1$. From left to right column, $t = 0.2$, 0.4, and 0.6, respectively.

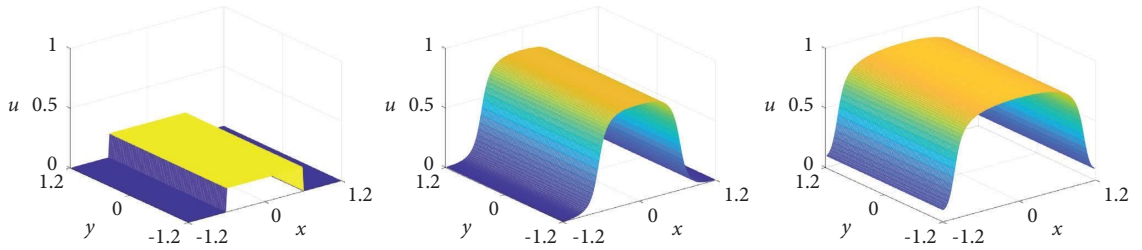

(a)

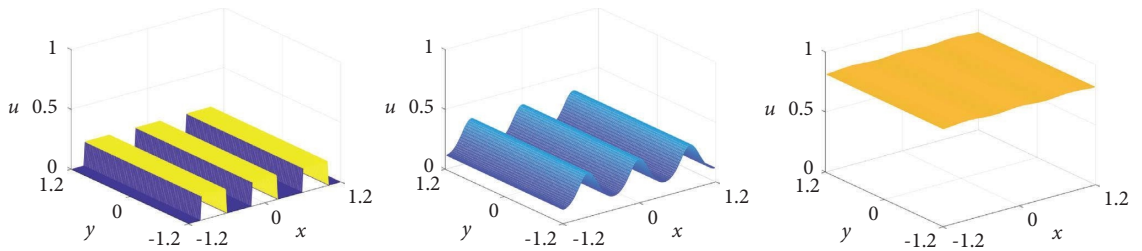

(b)

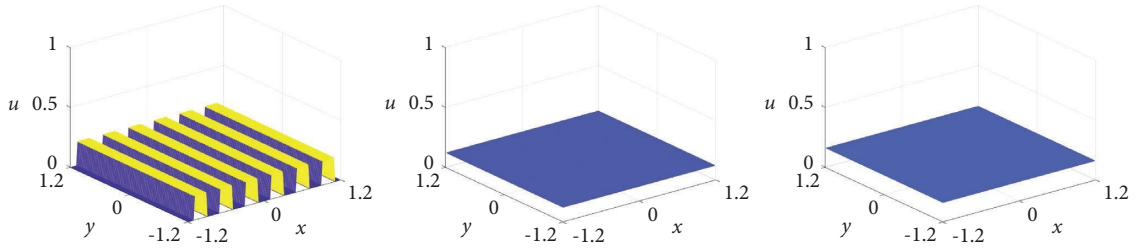

(c)

Figure 11: Continued.

1469, 2023, 1, Downloaded from https://onlinelibrary.wiley.com/doi/10.1155/2023/5527728 by Junseok Kim - Korea University Medical , Wiley Online Library on [14/07/2025]. See the Terms and Conditions (https://onlinelibrary.wiley.com/terms-and-conditions) on Wiley Online Library for rules of use; OA articles are governed by the applicable Creative Commons License

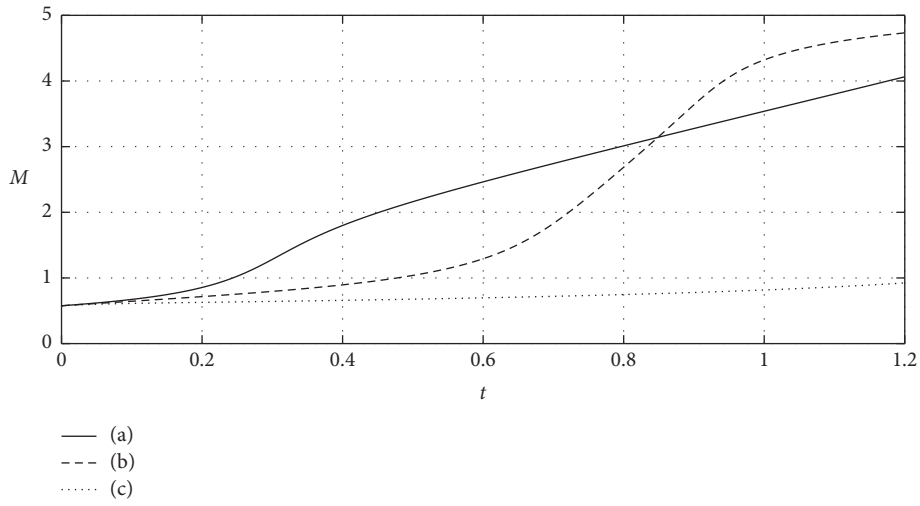

(d)

FIGURE 11: (a–c) are evolutions of initial conditions equations (26)–(28), respectively. From left to right, times are at $t = 0, 60\Delta t$, and $120\Delta t$. (d) Temporal evolution of total mass: (a) solid line, (b) dashed line, and (c) dotted line.

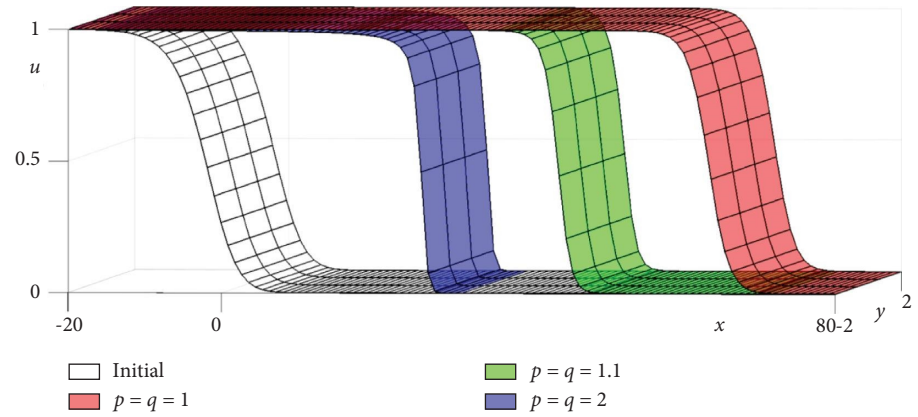

FIGURE 12: Traveling wave solutions with various p and q values.

Here, $p = q = 5$, $D = 0.05$, $N_x = N_y = 120$, $\Delta t = 0.01$, and final time $T = 1.2$ are used. In Figure 11, (a)–(c) are the evolutions of initial conditions equations (26)–(28), respectively. From left to right, times are at $t = 0, 60\Delta t$, and $120\Delta t$. (d) is the temporal evolution of total mass: (a) solid line, (b) dashed line, and (c) dotted line. In Figure 11(a), the solution of equation (27) grows faster than equations (28) and (29) at first. However, the solution grows more slowly than that of equation (28) over time. In Figure 11(b), it can be seen that the solution grows rapidly after evolution has progressed to some extent.

3.6. Traveling Wave Solution. Finally, we investigate the traveling wave solution for various p and q values. We use the following initial condition on the $\Omega = (-20, 80) \times (-2, 2)$:

$$u(x, y, 0) = \left[\frac{1}{2} - \frac{1}{2}\tanh\left(\frac{x}{2\sqrt{6}}\right)\right]^2. \tag{30}$$

The parameters are $N_x = 1000$, $N_y = 40$, $T = 8$, $\Delta t = 0.01$, and $D = 1$. Figure 12 shows the initial condition and final time solutions with different p and q values. We can observe the sharp transition layer as the values of p and q increase because of the narrow curve shape of the nonlinear term in the governing equation.

The wave speed of traveling wave solution is calculated and compared with the exact solution. For comparison with the exact solution of the traveling wave solution, we consider the case $p = q = 1$. The exact solution of traveling wave solution is as follows:

$$u(x, y, t) = \left[\frac{1}{2} - \frac{1}{2}\tanh\left(\frac{1}{2\sqrt{6}}\left(x - \frac{5t}{\sqrt{6}}\right)\right)\right]^2, \tag{31}$$

with the wave speed $s = 5/\sqrt{6}$. In order to numerically obtain the wave speed, the numerical solution is obtained when $t = 10$ in the domain $\Omega = (-20, 40) \times (-0.5, 0.5)$ to obtain the wave speed. The parameters used are $h = 0.025$ and $\Delta t = h^2$. The numerical wave speed is 2.0407 and when compared

1469, 2023, 1, Downloaded from https://onlinelibrary.wiley.com/doi/10.1155/2023/5527728 by Junseok Kim - Korea University Medical , Wiley Online Library on [14/07/2025]. See the Terms and Conditions (https://onlinelibrary.wiley.com/terms-and-conditions) on Wiley Online Library for rules of use; OA articles are governed by the applicable Creative Commons License

with s, the difference is 4.9975e − 4, which confirms that the numerical wave speed is appropriate.

4. Discussion and Conclusions

In this article, we developed an unconditionally stable computational scheme for the modified Fisher–KPP equation modeling population dynamics in 2D space. The Fisher–KPP equation models the process of interaction between reaction and diffusion. The proposed novel numerical solution algorithm consists of an ADI scheme and an interpolation method. The proposed numerical scheme is temporally and spatially second-order accurate. We confirmed the performance of the proposed method through numerical tests such as convergence and stability tests and the effects of model parameters and initial conditions. In future work, we use a second-order unconditionally energy stable time-marching scheme [45] to solve the Fisher–KPP equation.

Data Availability

No underlying data were collected or produced in this study.

Conflicts of Interest

The authors declare that they have no conflicts of interest.

Authors' Contributions

Soobin Kwak conceptualized the study, curated the data, performed formal analysis and investigation, and was responsible for methodology. Soobin Kwak was responsible for software, validation, visualization, writing the original draft, and writing, reviewing, and editing. Seungyoon Kang curated the data, performed formal analysis, investigation, software, and writing, reviewing, and editing. Seokjun Ham performed formal analysis, investigation, methodology, software, validation, visualization, writing–original draft, writing, reviewing, and editing. Youngjin Hwang methodology, visualizations, writing the original draft, and writing, reviewing, and editing. Gyeonggyu Lee was responsible for methodology, visualization, writing, reviewing, and editing. Junseok Kim conceptualized the study; performed formal analysis; and participated in funding acquisition, investigation, methodology, project administration, software, supervision, validation, writing the original draft, and writing, reviewing, and editing.

Acknowledgments

The corresponding author (J.S. Kim) was supported by the Brain Korea 21 FOUR from the Ministry of Education of Korea.

References

[1] R. A. Fisher, "The wave of advance of advantageous genes," *Annals of Eugenics*, vol. 7, no. 4, pp. 355–369, 1937.

[2] R. B. Salako and W. Shen, "Long time behavior of random and nonautonomous Fisher–KPP equations: Part I-Stability of Equilibria and Spreading Speeds," *Journal of Dynamics and Differential Equations*, vol. 33, no. 2, pp. 1035–1070, 2020.

[3] G. Tian, H. Wang, and Z. Wang, "Spreading speed in the Fisher–KPP equation with nonlocal delay," *Acta Mathematica Scientia*, vol. 41, no. 3, pp. 875–886, 2021.

[4] J. F. Leyva and R. G. Plaza, "Spectral stability of traveling fronts for reaction diffusion-degenerate Fisher–KPP equations," *Journal of Dynamics and Differential Equations*, vol. 32, no. 3, pp. 1311–1342, 2020.

[5] E. Hernández and S. Trofimchuk, "Nonstandard quasi-monotonicity: an application to the wave existence in a neutral KPP–Fisher equation," *Journal of Dynamics and Differential Equations*, vol. 32, no. 2, pp. 921–939, 2020.

[6] C. Feng, M. A. Lewis, C. Wang, and H. Wang, "A Fisher–KPP model with a nonlocal weighted free boundary: analysis of how habitat boundaries expand, balance or shrink," *Bulletin of Mathematical Biology*, vol. 84, no. 3, pp. 34–27, 2022.

[7] D. J. Warne, R. E. Baker, and M. J. Simpson, "Using experimental data and information criteria to guide model selection for reaction-diffusion problems in mathematical biology," *Bulletin of Mathematical Biology*, vol. 81, no. 6, pp. 1760–1804, 2019.

[8] F. Bonizzoni, M. Braukhoff, A. Jüngel, and I. Perugia, "A structure-preserving discontinuous Galerkin scheme for the Fisher–KPP equation," *Numerische Mathematik*, vol. 146, no. 1, pp. 119–157, 2020.

[9] M. Braukhoff, I. Perugia, and P. Stocker, "An entropy structure preserving space-time formulation for cross-diffusion systems: analysis and Galerkin discretization," *SIAM Journal on Numerical Analysis*, vol. 60, no. 1, pp. 364–395, 2022.

[10] J. M. Roquejoffre and V. Roussier-Michon, "Nontrivial dynamics beyond the logarithmic shift in two-dimensional Fisher–KPP equations," *Nonlinearity*, vol. 31, no. 7, pp. 3284–3307, 2018.

[11] B. Yahyaoui, M. Ayadi, and A. Habbal, "Fisher–KPP with time dependent diffusion is able to model cell-sheet activated and inhibited wound closure," *Mathematical Biosciences*, vol. 292, pp. 36–45, 2017.

[12] N. Ozdemir, A. Secer, and M. Bayram, "An algorithm for numerical solution of some nonlinear multi-dimensional parabolic partial differential equations," *Journal of Computational Science*, vol. 56, Article ID 101487, 2021.

[13] A. Secer and M. Cinar, "A Jacobi wavelet collocation method for fractional Fisher's equation in time," *Thermal Science*, vol. 24, no. 1, pp. 119–129, 2020.

[14] W. Rui and H. Zhang, "Separation variable method combined with integral bifurcation method for solving time-fractional reaction-diffusion models," *Computational and Applied Mathematics*, vol. 39, no. 4, pp. 1–26, 2020.

[15] M. Z. Youssef, M. M. Khader, I. Al-Dayel, and W. E. Ahmed, "Solving fractional generalized Fisher–Kolmogorov–Petrov sky–Piskunov's equation using compact-finite different methods together with spectral collocation algorithms," *Journal of Mathematics*, vol. 2022, Article ID 1901131, 9 pages, 2022.

[16] M. Modanli and B. Bajjah, "Double laplace decomposition method and finite difference method of time-fractional Schrödinger pseudoparabolic partial differential equation with Caputo derivative," *Journal of Mathematics*, vol. 2021, Article ID 7113205, 10 pages, 2021.

[17] K. Minors and J. H. P. Dawes, "Invasions slow down or collapse in the presence of reactive boundaries," *Bulletin of Mathematical Biology*, vol. 79, no. 10, pp. 2197–2214, 2017.

[18] J. L. D. Palencia, "Analysis of selfsimilar solutions and a comparison principle for an heterogeneous diffusion cooperative system with advection and non-linear reaction,"

1469, 2023, 1, Downloaded from https://onlinelibrary.wiley.com/doi/10.1155/2023/5527728 by Junseok Kim - Korea University Medical , Wiley Online Library on [14/07/2025]. See the Terms and Conditions (https://onlinelibrary.wiley.com/terms-and-conditions) on Wiley Online Library for rules of use; OA articles are governed by the applicable Creative Commons License

Computational and Applied Mathematics, vol. 40, no. 8, pp. 302–320, 2021.

[19] L. Girardin, "Two components is too simple: an example of oscillatory Fisher–KPP system with three components," *Proceedings of the Royal Society of Edinburgh: Section A Mathematics*, vol. 150, no. 6, pp. 3097–3120, 2020.

[20] B. Lou and J. Lu, "Spreading in a cone for the Fisher–KPP equation," *Journal of Differential Equations*, vol. 267, no. 12, pp. 7064–7084, 2019.

[21] J. M. Roquejoffre and A. Tarfulea, "Gradient estimates and symmetrization for Fisher–KPP front propagation with fractional diffusion," *Journal de Mathematiques Pures et Appliquees*, vol. 108, no. 4, pp. 399–424, 2017.

[22] F. Flandoli, L. Galeati, and D. Luo, "Delayed blow-up by transport noise," *Communications in Partial Differential Equations*, vol. 46, no. 9, pp. 1757–1788, 2021.

[23] M. Khater and A. M. Alabdali, "Multiple novels and accurate traveling wave and numerical solutions of the (2+1) dimensional Fisher-Kolmogorov- petrovskii-piskunov equation 2+1 dimensional Fisher–Kolmogorov–petrovskii–Piskunov equation," *Mathematics*, vol. 9, no. 12, p. 1440, 2021.

[24] S. W. McCue, W. Jin, T. J. Moroney, K. Y. Lo, S. E. Chou, and M. J. Simpson, "Hole-closing model reveals exponents for nonlinear degenerate diffusivity functions in cell biology," *Physica D: Nonlinear Phenomena*, vol. 398, pp. 130–140, 2019.

[25] Ö. Oruç, "An efficient wavelet collocation method for nonlinear two-space dimensional Fisher–Kolmogorov–Petrovsky–Piscounov equation and two-space dimensional extended Fisher–Kolmogorov equation," *Engineering with Computers*, vol. 36, no. 3, pp. 839–856, 2020.

[26] G. Faye and M. Holzer, "Asymptotic stability of the critical Fisher–KPP front using pointwise estimates," *Zeitschrift für Angewandte Mathematik und Physik*, vol. 70, no. 1, pp. 13–21, 2019.

[27] W. B. Xu, W. T. Li, and S. Ruan, "Spatial propagation in nonlocal dispersal Fisher–KPP equations," *Journal of Functional Analysis*, vol. 280, no. 10, Article ID 108957, 2021.

[28] R. D. Benguria, M. C. Depassier, and S. Rica, "Variational estimates for the speed propagation of fronts in a nonlinear diffusive Fisher equation," *Chaos, Solitons and Fractals*, vol. 164, no. 2022, Article ID 112668, 2022.

[29] G. G. Piva, E. H. Colombo, and C. Anteneodo, "Interplay between scales in the nonlocal FKPP equation," *Chaos, Solitons and Fractals*, vol. 153, Article ID 111609, 2021.

[30] M. M. Khater, M. S. Mohamed, and R. A. Attia, "On semi analytical and numerical simulations for a mathematical biological model; the time-fractional nonlinear Kolmogorov–Petrovskii–Piskunov (KPP) equation," *Chaos, Solitons and Fractals*, vol. 144, Article ID 110676, 2021.

[31] A. G. Bratsos and A. Q. M. Khaliq, "An exponential time differencing method of lines for Burgers–Fisher and coupled Burgers equations," *Journal of Computational and Applied Mathematics*, vol. 356, pp. 182–197, 2019.

[32] J. E. Macías-Díaz and A. Gallegos, "On a positivity-preserving numerical model for a linearized hyperbolic Fisher–Kolmogorov–Petrovski–Piscounov equation," *Journal of Computational and Applied Mathematics*, vol. 354, pp. 603–611, 2019.

[33] R. Jiwari, "Local radial basis function-finite difference based algorithms for singularly perturbed Burgers' model," *Mathematics and Computers in Simulation*, vol. 198, pp. 106–126, 2022.

[34] S. Pandit, "Local radial basis functions and scale-3 Haar wavelets operational matrices based numerical algorithms for generalized regularized long wave model," *Wave Motion*, vol. 109, Article ID 102846, 2022.

[35] S. Pandit and R. C. Mittal, "A numerical algorithm based on scale-3 Haar wavelets for fractional advection dispersion equation," *Engineering Computations*, vol. 38, no. 4, pp. 1706–1724, 2021.

[36] R. Jiwari, R. Jiwari, and N. Kumar, "Analysis and simulation of Korteweg-de Vries–Rosenau-regularised long-wave model via Galerkin finite element method," *Computers and Mathematics with Applications*, vol. 135, pp. 134–148, 2023.

[37] R. C. Harwood, *Operator Splitting Method and Applications for Semilinear Parabolic Partial Differential Equations*, Washington State University, Washington, DC, USA, 2011.

[38] M. Izadi, "Split-step finite difference schemes for solving the nonlinear Fisher equation," *J. Mahani Math. Res.*, vol. 7, no. 1, pp. 37–55, 2018.

[39] W. Dai, "A generalized Peaceman–Rachford ADI scheme for solving two-dimensional parabolic differential equations," *Journal of Scientific Computing*, vol. 12, pp. 353–360, 1997.

[40] J. Sheldon and L. H. Thomas, "The use of large scale computing in physics," *Journal of Applied Physics*, vol. 24, no. 3, pp. 235–242, 1953.

[41] S. Kim, C. Lee, H. G. Lee et al., "An unconditionally stable positivity-preserving scheme for the one-dimensional Fisher–Kolmogorov–Petrovsky–Piskunov equation," *Discrete Dynamics in Nature and Society*, vol. 2021, Article ID 7300471, 11 pages, 2021.

[42] C. Lee, H. Kim, S. Yoon et al., "An unconditionally stable scheme for the Allen–Cahn equation with high-order polynomial free energy," *Communications in Nonlinear Science and Numerical Simulation*, vol. 95, Article ID 105658, 2021.

[43] H. G. Lee and J. Y. Lee, "A second order operator splitting method for Allen–Cahn type equations with nonlinear source terms," *Physica A: Statistical Mechanics and Its Applications*, vol. 432, pp. 24–34, 2015.

[44] Y. Li, D. Jeong, J. Shin, and J. Kim, "A conservative numerical method for the Cahn–Hilliard equation with Dirichlet boundary conditions in complex domains," *Computers and Mathematics with Applications*, vol. 65, no. 1, pp. 102–115, 2013.

[45] J. Wu, J. Yang, and Z. Tan, "Highly efficient and fully decoupled BDF time-marching schemes with unconditional energy stabilities for the binary phase-field crystal models," *Engineering with Computers*, vol. 5, pp. 1–25, 2022.

1469, 2023, 1, Downloaded from https://onlinelibrary.wiley.com/doi/10.1155/2023/5527728 by Junseok Kim - Korea University Medical , Wiley Online Library on [14/07/2025]. See the Terms and Conditions (https://onlinelibrary.wiley.com/terms-and-conditions) on Wiley Online Library for rules of use; OA articles are governed by the applicable Creative Commons License